

# XMM-Newton Observation and Optical Monitoring of the Candidate Redback Millisecond Pulsar 1FGL J0523.5–2529

JULES P. HALPERN<sup>1</sup> AND SLAVKO BOGDANOV<sup>2</sup>

<sup>1</sup>*Department of Astronomy, Columbia University, 550 West 120th Street, New York, NY 10027-6601, USA*

<sup>2</sup>*Columbia Astrophysics Laboratory, Columbia University, 550 West 120th Street, New York, NY 10027-6601, USA*

## ABSTRACT

1FGL J0523.5–2529 is a Fermi selected redback millisecond pulsar candidate that exhibited luminous optical and X-ray flares in 2020–2021. We obtained a simultaneous X-ray and *U*-band observation with XMM-Newton in 2025, the first to cover the 16.5 hr orbit of 1FGL J0523.5–2529. The X-ray luminosity was in an intermediate state with a power-law photon spectral index of  $\Gamma = 1.53 \pm 0.02$ . Frequent flares were superposed on a broad, single-peaked modulation, the latter characteristic of intrabinary shock models in which the shock front is wrapped around the pulsar. We speculate that density enhancements in the shocked companion wind cause flares, as well as variable optical recombination lines. The *U*-band light curve was dominated by ellipsoidal modulation of the nearly Roche lobe filling companion star, similar to that seen in ground-based optical photometry. We also used this effect in 10 years of ATLAS monitoring to improve the precision of the orbital period to 0.6881366(19) days. Considering that searches for radio pulsations from 1FGL J0523.5–2529 at all orbital phases have been unsuccessful, the shocked wind usually surrounds the pulsar.

*Unified Astronomy Thesaurus concepts:* Millisecond pulsars (1062); Binary pulsars (153); Radio pulsars (1353); Rotation-powered pulsars (1408); Pulsars (1306); Neutron stars (1108)

## 1. INTRODUCTION

The majority of millisecond pulsars (MSPs) have either a white dwarf or a low-mass, evolved star as a companion. The canonical explanation for the origin of MSPs is “recycling” of the neutron star by accretion during a low-mass X-ray binary (LMXB) phase (Alpar et al. 1982; Radhakrishnan & Srinivasan 1982), after which radio pulsations turn on because accretion has stopped. A highlight of the Fermi mission is its discovery of many  $\gamma$ -ray-emitting black widows (BWs) and redbacks, previously rare radio MSPs in which the relativistic pulsar wind heats and ablates the photosphere of a companion star. BWs have orbital periods  $\leq 1$  day and degenerate companions of  $< 0.05 M_{\odot}$ , while redbacks have non-degenerate  $0.1 - 1 M_{\odot}$  companions that are generally hotter and less dense than main-sequence stars of the same mass. Koljonen & Linares (2025) cataloged 50 BWs and 30 redbacks in the Galactic field (not including those in globular clusters). In addition, they list five BW candidates and 23 redback candidates from which pulsations have not yet been found.

Redback companions are close to filling their Roche lobes (Strader et al. 2019). Their winds can obscure the radio pulsar signal for a large fraction of the orbit (e.g., Deneva et al. 2021; Perez et al. 2023; Thongmearkom

et al. 2024), and sometimes produce optical emission lines. Nonthermal emission from redbacks is attributed to shocks from the collision between the pulsar and stellar winds and is dominant in X-rays (Al Noori et al. 2018; Bogdanov et al. 2005, 2011, 2014). X-ray flux is usually modulated around the orbit, which is interpreted in terms of the geometry of the intrabinary shock, with synchrotron emission beamed by particles moving tangentially to the shock surface (Romani & Sanchez 2016; Wadiasingh et al. 2017, 2018; Kandel et al. 2019; van der Merwe et al. 2020; Cortés & Sironi 2022, 2024, 2025).

The photosphere of the companion can be heated by the high-energy photons produced by the shock or directly by pulsar wind particles (Sanchez & Romani 2017). The optical modulation observed around the orbit is sometimes dominated by this heating effect. Alternatively, when heating is weak, intrinsic ellipsoidal modulation of light from the tidally distorted, nearly Roche-lobe-filling star is the main contributor (Li et al. 2014; Bellm et al. 2016; van Staden & Antoniadis 2016; Shahbaz et al. 2017), with large starspots also possibly playing a role. All of these effects can vary. Photospheric heating patterns change over weeks and months. In several redbacks minutes-long flares increase the luminosity by a factor of 10–100 in X-rays, and up to  $\sim 1$  magnitude in optical, e.g., in

PSR J1048+2339 (Cho et al. 2018), PSR J0838–2827 (=3FGL J0838.8–2829; Halpern et al. 2017a; Rea et al. 2017), and 4FGL J1838.2+3223 (Zyuzin et al. 2024).

The subject of this paper is 1FGL J0523.5–2529, the first candidate redback to be identified (Strader et al. 2014), in this case from an X-ray counterpart in Swift and an optical light curve consistent with pure elliptical modulation with a period of 15.6 hr in the Catalina Real-Time Transient Survey data (CRTS; Drake et al. 2009). Radio pulsations have not been detected from this source despite extensive searches (Thongmearkom et al. 2024; Johnson et al. 2025). Spectroscopy of the early K star measured its orbital velocity and rotational broadening (Strader et al. 2014), indicating a mass ratio of  $0.61 \pm 0.06$  and a companion star mass in the range  $0.8 - 1.3 M_{\odot}$ , the largest among redbacks. These parameters require an orbital inclination in the range  $57^{\circ} < i < 80^{\circ}$ . We assume a distance of 2.24 kpc from the Gaia measured parallax of  $0.446 \pm 0.042$  mas in its extended third data release (EDR3; Gaia Collaboration et al. 2021).

In early 2020, we discovered dramatic optical flaring from 1FGL J0523.5–2529 and carried out a Swift campaign (Halpern et al. 2022, hereafter Paper 1) that detected simultaneous X-ray and optical/UV flares. Flares were also associated with the emergence of optical emission lines. The flares had rise times of a few minutes, sometimes recurred for hours or days, and continued intermittently through 2021. A wide range of X-ray luminosity was observed during the campaign, spanning a factor of  $\approx 100$  between a barely detected minimum and the peak of the brightest flare.

Here we present continued ground-based optical monitoring through early 2026, together with results from an XMM-Newton pointing, the first X-ray observation sensitive to the non-flaring state and to cover a full 16.5 hr binary orbit. Section 2 presents the optical time-series data from the MDM Observatory and monitoring data from the Zwicky Transient Facility (ZTF; Bellm et al. 2019) and the Asteroid Terrestrial-impact Last Alert System (ATLAS; Tonry et al. 2018). The XMM-Newton observation is described in Section 3. The results are discussed and interpreted in Section 4. The main conclusions are summarized in Section 5.

## 2. OPTICAL OBSERVATIONS

### 2.1. MDM Observatory 1.3 m and ZTF

We used the MDM Observatory 1.3 m McGraw-Hill telescope on Kitt Peak for time-series photometry of 1FGL J0523.5–2529 in the  $r$  band for 20 nights over seven observing runs in 2023–2026, as listed in Table 1. The methods are identical to those used in Paper 1.

**Table 1.** Log of MDM  $r$ -band Time-series Photometry

Date	Exp.	$N_{\text{exp}}$	Time	Phase
(UT)	(s)		(UTC)	( $\phi$ )
2023 Jan 23	60	68	01:40–02:54	0.991–0.066
2023 Jan 25	60	185	01:40–04:53	0.897–0.093
2023 Jan 28	60	85	01:40–03:09	0.257–0.347
2023 Nov 7	60	366	06:32–12:58	0.809–0.198
2023 Nov 8	60	366	06:31–12:57	0.261–0.650
2023 Nov 9	60	99	06:24–08:07	0.707–0.811
2023 Nov 10	60	174	06:20–09:22	0.155–0.339
2023 Nov 11	60	171	06:14–09:13	0.603–0.783
2024 Nov 5	60	341	06:36–12:34	0.777–0.138
2024 Nov 6	60	265	06:41–11:19	0.235–0.516
2024 Nov 7	60	347	06:53–12:58	0.700–0.069
2024 Nov 8	60	357	06:22–12:38	0.123–0.502
2025 Jan 26	60	85	02:49–04:17	0.709–0.798
2025 Jan 27	60	148	01:39–04:14	0.092–0.248
2025 Jan 28	60	117	01:36–03:38	0.542–0.665
2025 Sep 29	60	197	09:10–12:36	0.579–0.787
2025 Dec 20	60	367	03:44–10:09	0.416–0.805
2025 Dec 21	60	365	03:46–10:09	0.871–0.258
2026 Jan 20	60	369	01:41–08:10	0.339–0.733
2026 Jan 21	60	344	01:58–08:00	0.811–0.175

A thinned, backside-illuminated SITe CCD (Templeton) was windowed to achieve an efficient read/prep cycle time of 3 s in between 60 s exposures. The times were converted to TDB using the online tool<sup>3</sup> of Eastman et al. (2010) and the Gaia-CRF3 position R.A.=05<sup>h</sup>23<sup>m</sup>16<sup>s</sup>.931, decl.=−25°27′37″13 (Gaia Collaboration et al. 2021), which is referenced for proper motion to epoch 2016.0.

Differential photometry was performed with respect to the PanSTARRS magnitude of a nearby comparison star, the long-term stability of which was verified in ATLAS and ZTF data. Figure 1 shows the resulting photometry folded in the orbital ephemeris described in Section 2.3. Due to the 16.5 hr orbital period and southerly declination of 1FGL J0523.5–2529, it is possible to cover at most 0.4 cycles per night from Kitt Peak; a five-night span, which was rarely available, is needed to sample all phases.

As in Paper 1, an analytic model of ellipsoidal modulation (Morris & Naftilan 1993; Gomel et al. 2021) is

<sup>3</sup> <https://astrutils.astronomy.osu.edu/time/utc2bjd.html>

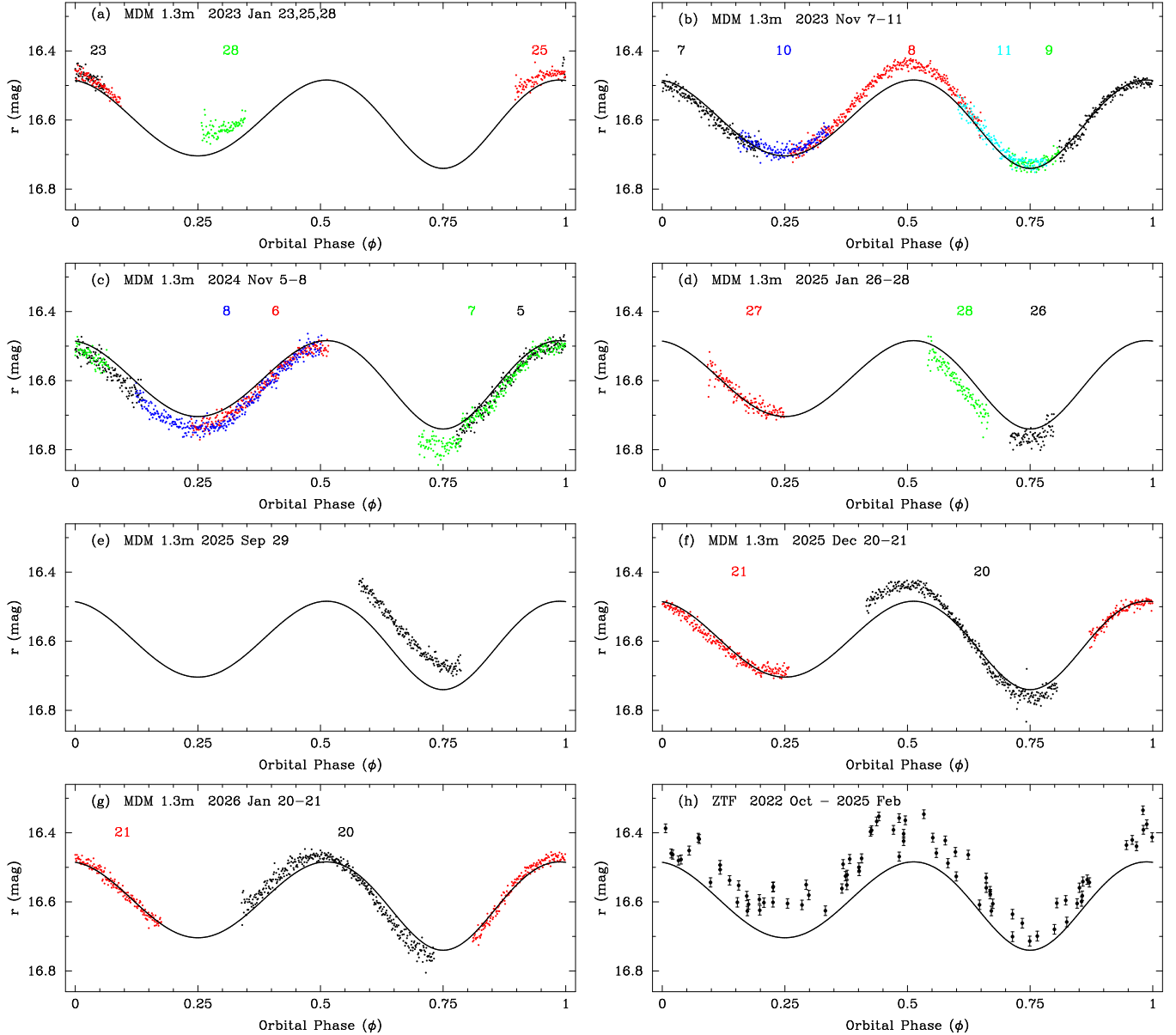


**Figure 1.** Panels a–g:  $r$ -band time-series photometry of 1FGL J0523.5–2529 during seven runs on the MDM 1.3 m from 2023 to 2026, folded according to the orbital ephemeris described in Section 2.3. A log of these observations is given in Table 1. The data points are color coded and labeled by the day of the month. A fixed model of ellipsoidal modulation (not a fit to the data) is superposed as an aid to visualizing deviations and variability. Panel h is the ZTF  $r$ -band data from an overlapping period, which is consistent with the MDM data except for an apparent  $\approx 0.07$  mag offset in calibration.

superposed on the light curves. The orbital inclination  $i = 67^\circ$  and the mass ratio  $q = 0.61$  come from the spectroscopic study by Strader et al. (2014), while Roche-lobe filling factor  $f = 0.99$ , linear limb-darkening coefficient 0.65, and gravity-darkening coefficient 0.45 are assumed. The two coefficients are suitable for an atmosphere of  $T_{\text{eff}} = 5,000$  K and  $\log g = 4.0$  (Claret & Bloemen 2011; Torres 2021). The curve is not a fit to the data, but a template to illustrate a variety of deviations from the model, which might be attributable

to asymmetric and variable photospheric heating of the companion star’s photosphere by the pulsar and intrabinary wind shock. We also display 85  $r$ -band data points in 2022–2025 from the ZTF 24th data release, which largely overlap in time with the MDM observations and match the ellipsoidal model to first order except for a possible  $\approx 0.07$  mag offset in calibration.

## 2.2. ATLAS

We downloaded ATLAS forced photometry of 1FGL J0523.5–2529, which is the densest long-term op-

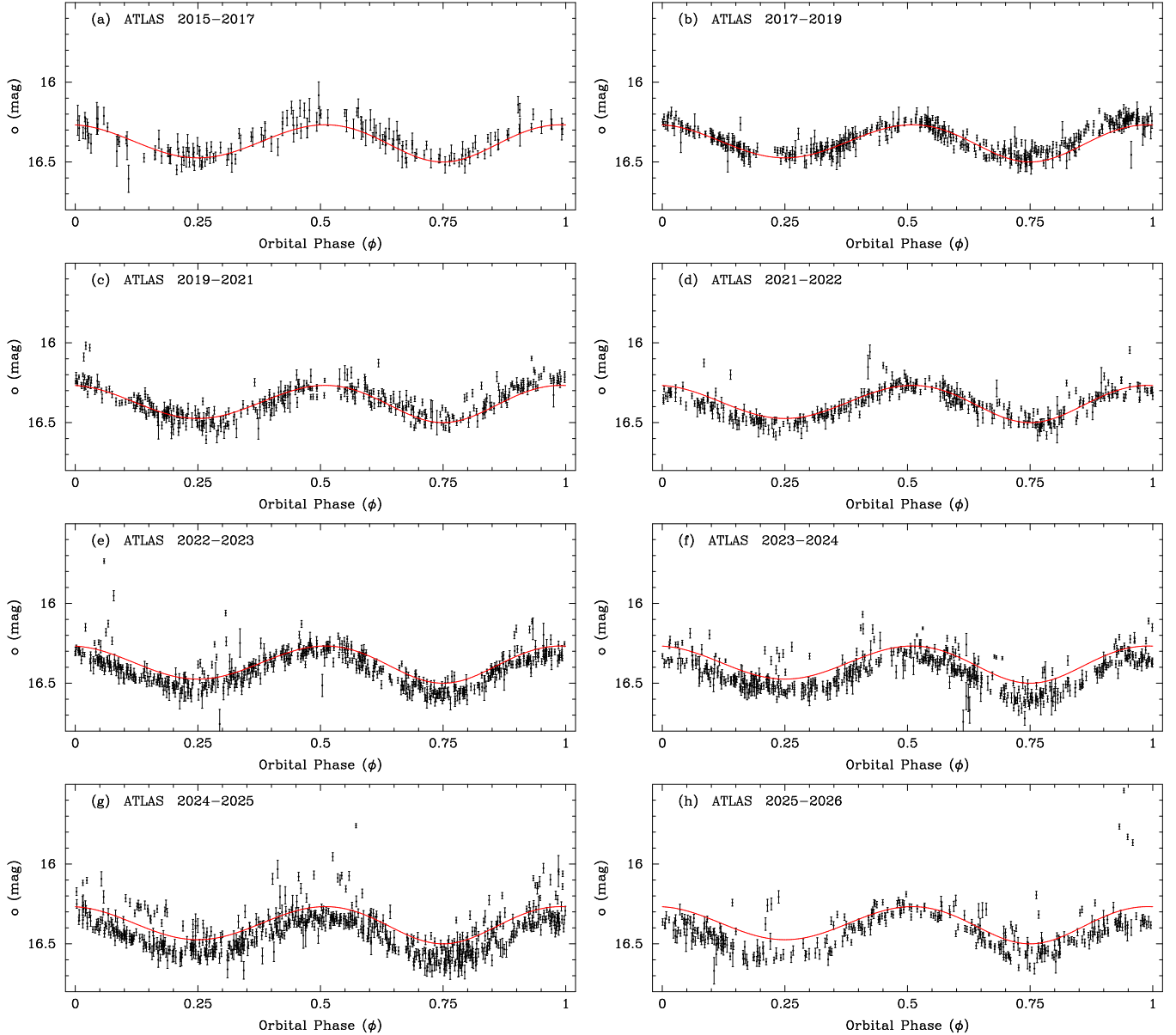


**Figure 2.** ATLAS forced photometry in the  $o$  filter folded according to the orbital ephemeris described in Section 2.3. Each panel contains either one or two observing seasons. A fixed model of ellipsoidal modulation (not a fit to the data) is superposed as an aid to visualizing deviations and long-term variability.

tical record of this source. After applying conservative quality filters<sup>4</sup> and removing points with uncertainties  $> 0.1$  mag, there are 3522 observations in the “orange”  $o$  filter (560–820 nm) and 946 points in the “cyan”  $c$  filter (420–650 nm) spanning 2015 October 8 to 2026 January 17. The  $o$  points in Figure 2 are grouped into one or two observing seasons per panel. The same ellipsoidal model as above is used as a fiducial marker of long-term variability. Gradual fading by  $\approx 0.15$  mag over 10 years

is seen in both the  $o$  and  $c$  filters. The same trend is present in the ZTF  $r$  and  $g$  filters (from 2018 to 2025, not shown here), with a slight increase in  $g - r$ .

There are a number of outlying points that may be indicative of flares such as those documented in Paper 1 from high-cadence MDM data. Since ATLAS takes four 30 s exposures of each field within a 1 hr period, flares may be confirmed by more than one detection in the sequence of four. We have not examined all of the high points in detail, but a notable example of a probable flare occurs in Figure 2h, where all four high points

<sup>4</sup> <https://fallingstar-data.com/forcedphot/faq/>

around phase 0.95 were taken over a span of 27 minutes beginning on 2025 November 29 04:16:58 UT.

### 2.3. Updated Orbital Ephemeris

The original spectroscopic ephemeris developed in 2013–2014 (Strader et al. 2014) is still the only one published:  $P = 0.688134 \pm 0.000028$  day,  $T_{0.75} = 2456577.64636 \pm 0.0037$  (BJD). Here  $T_{0.75}$  is the epoch of superior conjunction of the companion star, which occurs at phase  $\phi = 0.75$  in the radio pulsar convention, where  $\phi = 0$  is the ascending node of the pulsar. The times of extrema of the optical light curves from 2020–2021 in Paper 1 were adequately matched by the simple ellipsoidal model using this ephemeris. Nevertheless, considering the significant deviations of the light curve from the simple model, there is a systematic ambiguity in the phase of the photometric extrema relative to the spectroscopic epoch that is larger than the  $\approx 5$  minute precision of the latter. Therefore, we choose the spectroscopic (kinematic) epoch as the fiducial point to define the phases of the X-ray and optical light curves. However, the uncertainty of the original spectroscopic orbital period extrapolates to a large expected error of  $\approx 0.18$  cycles at the epoch of the XMM-Newton observation.

Fortunately, the 10 yr span of the ATLAS data set affords a significant improvement in the precision of the orbital period. For this purpose, we applied a Lomb-Scargle periodogram to the data in Figure 2, excluding points with  $o \leq 16.1$  or  $o > 16.7$ . Noting that nearly all power is in the first harmonic due to the double-peaked wave form, we use the harmonic to get  $P = 0.6881366(19)$  days for the orbital period, an order-of-magnitude refinement that is fortuitously close to the original value. This is the average period over the 10-yr span. Although it is known from radio and  $\gamma$ -ray pulse timing that the orbital periods of redbacks change stochastically on timescales of years, this only appears as drifts in the time of ascending node by tens of seconds (e.g., Deneva et al. 2016; Thongmeearkom et al. 2024), an effect that is too small to be detected in the photometry. Adopting here a hybrid ephemeris consisting of the spectroscopic epoch and the ATLAS period, the propagated uncertainty in the phasing of the X-ray and optical light curves relative to the kinematic orbit is acceptably  $\approx 0.0126$  days (0.018 cycles).

## 3. XMM-Newton OBSERVATION

We observed 1FGL J0523.5–2529 with XMM-Newton for 61 ks on 2025 February 25. The EPIC pn (Strüder et al. 2001), MOS1, and MOS2 (Turner et al. 2001) cameras were used in the large window mode with the thin optical blocking filter. All three data sets were processed

with the Science Analysis Software (SAS) package version 22.1.0. The standard flag and pattern even screening criteria were applied. The XMM-Newton Optical Monitor (OM; Mason et al. 2001) was used with the *U* filter and a fast-mode window with a tracking frame duration of 20 s. A photometric light curve was extracted using the *omfchain* processing pipeline with the default parameter settings.

### 3.1. X-ray Spectrum

For spectral analysis, source events were extracted from a circular region of radius  $30''$  centered on the Gaia-CRF3 position. Background estimates were obtained from a source free region of radius  $60''$  in the vicinity of the source. The extracted pn and MOS1/2 source spectra were grouped such that each energy bin contains at least 25 counts. We account for absorption due to the interstellar medium using the *tbabs* model in XSPEC, which considers the VERN cross-sections (Verner et al. 1996) and WILM abundances (Wilms et al. 2000). We consider an absorbed power-law spectrum, which is expected from intra-binary shock emission.

The results of the spectroscopic analysis are summarized in Table 2 and are displayed in Figure 3. The best fit to the time-averaged spectrum gives a  $N_{\text{H}} = (1.4 \pm 0.5) \times 10^{20} \text{ cm}^{-2}$ , a photon index  $\Gamma = 1.53 \pm 0.02$ , and unabsorbed flux  $F_X = (5.48 \pm 0.07) \times 10^{-13} \text{ erg cm}^{-2} \text{ s}^{-1}$  in the 0.3–10 keV band, with  $\chi^2_{\nu} = 1.10$  for 474 degrees of freedom. All errors quoted are at the significance level  $1\sigma$ . For a distance of 2.24 kpc, the flux translates into a luminosity  $L_X = 3.3 \times 10^{32} \text{ erg s}^{-1}$ . The inferred hydrogen column density is consistent with the value of  $1.5 \times 10^{20} \text{ cm}^{-2}$  measured through the Galaxy towards 1FGL J0523.5–2529 (HI4PI Collaboration et al. 2016).

To examine any X-ray spectral variations over the binary orbit, we divide the data into two orbital phase segments 0.0–0.5 and 0.5–1 and fit a power-law spectrum to each separately. There is no appreciable change in the photon index between the two portions of the orbit (see Table 2).

### 3.2. X-ray and OM Light Curves

Background-subtracted light curves in the 0.2–10 keV range were created from each EPIC detector by extracting the source counts in a circle of radius  $20''$  and getting background counts from a circle of the same radius in a neighboring source-free region. The three light curves were merged in 200 s bins (Figure 4). It shows nearly continuous flaring superposed on a broad minimum centered around  $\phi = 0.25$  determined from the ephemeris described in Section 2.3. The X-ray light curve binned by 400 s is shown in Figure 5.

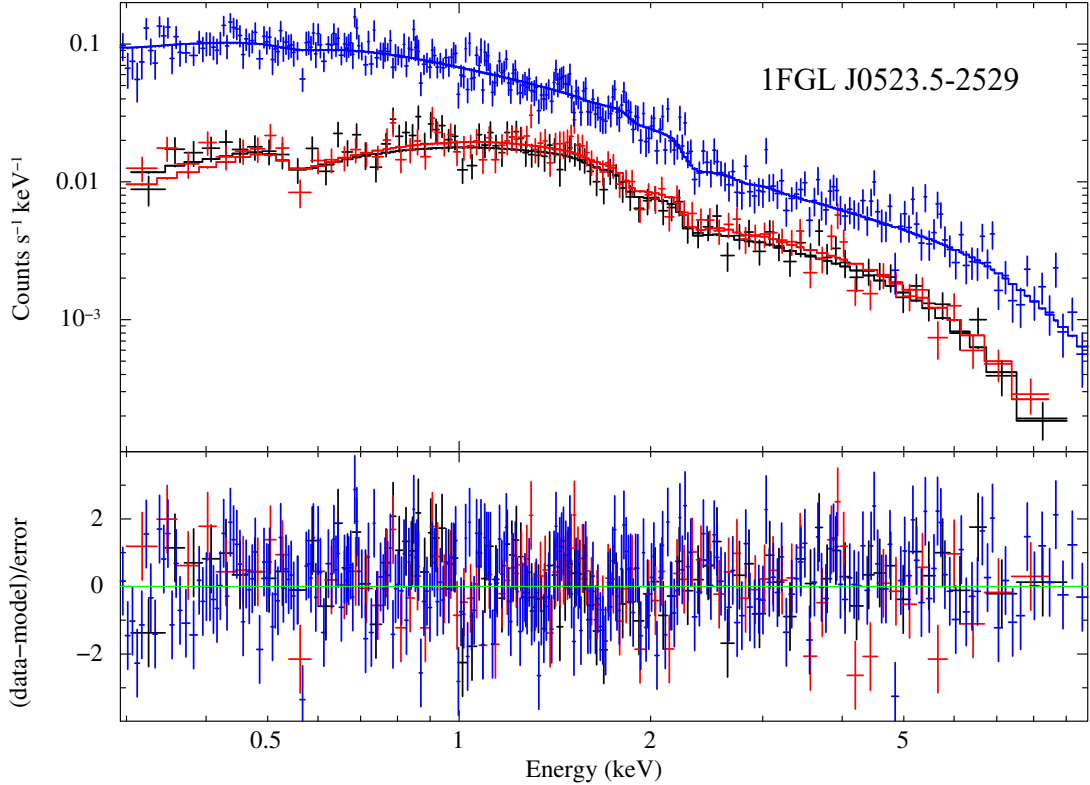


**Figure 3.** Total XMM-Newton spectrum and power-law fit, with pn data in blue and MOS in black and red. The bottom panel shows the residuals from the best fit.

**Table 2.** XMM-Newton Spectral Fits

Parameter	Orbital phase interval		
	0.0 – 1.0	0.0 – 0.5	0.5 – 1.0
$N_{\text{H}}$ ( $10^{20}$ $\text{cm}^{-2}$ )	$1.4 \pm 0.5$	$1.3 \pm 0.8$	$1.8 \pm 0.6$
$\Gamma$	$1.53 \pm 0.02$	$1.54 \pm 0.03$	$1.53 \pm 0.03$
PL norm. ( $10^{-5}$ $\text{keV}^{-1}$ $\text{cm}^{-2}$ $\text{s}^{-1}$ )	$6.78 \pm 0.13$	$5.38 \pm 0.16$	$8.16 \pm 0.20$
$F_X^a$ ( $10^{-13}$ $\text{erg cm}^{-2}$ $\text{s}^{-1}$ )	$5.48 \pm 0.07$	$4.33 \pm 0.09$	$6.60 \pm 0.11$
$\chi^2_{\nu}/\text{DoF}$	1.10/478	1.17/211	1.04/297

<sup>a</sup>Unabsorbed flux in the 0.3–10 keV range.

The OM light curve in Figure 4 was binned identically to the X-rays. The gap in the data is due to a telemetry drop that caused a telecommand failure of three of the 13 OM observations. Otherwise, it is broadly consistent with the ellipsoidal model except perhaps for some flaring around day 732.5. The parameters of the ellipsoid model are the same as those used for ground-based photometry except that the limb-darkening and gravity-darkening coefficients are 0.95 and 1.1, respectively, appropriate for the  $U$  band (Claret & Bloemen 2011).

## 4. DISCUSSION

### 4.1. Optical and X-ray Results

Bright flares such as those observed in the 2020–2021 MDM  $R$ -band observations of Paper 1 are not seen in the  $r$ -band light curves from 2023 to early 2026 presented here in Figure 1. Nevertheless, there is evidence of occasional flares in the more frequent but brief visits by ATLAS (Figure 2) during the latter period. Otherwise, the optical light curve of 1FGL J0523.5–2529 is dominated by ellipsoidal modulation. This also applies

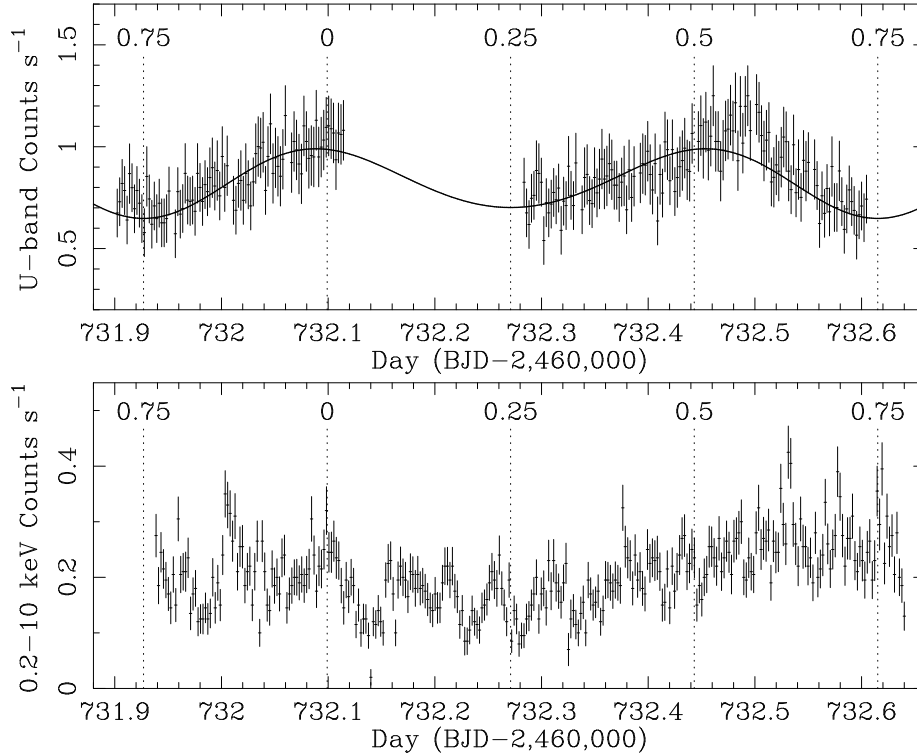


**Figure 4.** XMM-Newton light curves in 200 s bins, with orbital phases marked. Top: The gap in the OM data is due to a telemetry drop that caused a telecommand failure of three of the 13 OM observations. Otherwise, the light curve is broadly consistent with the ellipsoidal model except perhaps for some flaring around day 732.5. Bottom: Background subtracted and summed X-ray count rates from the pn and MOS detectors showing a broad minimum around phase 0.25 and nearly continuous flaring.

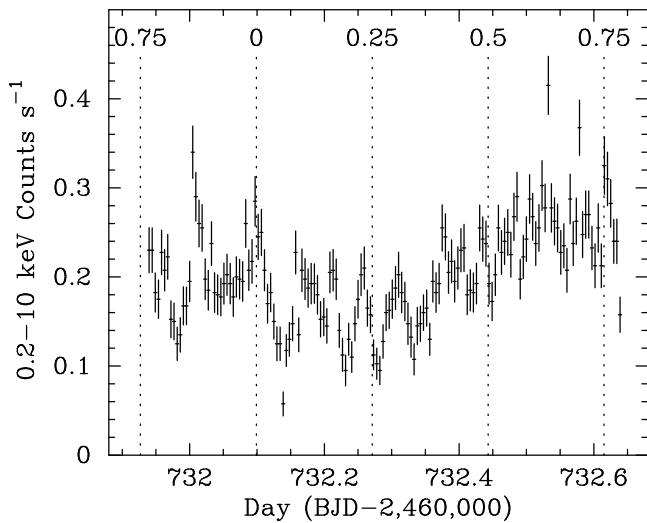


**Figure 5.** The X-ray light curve of Figure 4 in 400 s bins, with orbital phases marked.

to the OM  $U$  filter; only around phase 0.57 in Figure 4 is there a significant excess over the ellipsoidal model.

The zero point of the OM  $U$  filter in the AB magni-

tude system is 19.189 (corresponding to 1 counts  $s^{-1}$ )<sup>5</sup>. Therefore, the observed count rates ranging from 0.65 counts  $s^{-1}$  to 1.1 counts  $s^{-1}$  convert to  $U=19.66$ – $19.09$ , which is in excellent agreement with the folded Swift UVOT light curve in 2020 assembled from many brief observations (Paper 1). Only during the brightest flare on 2020 January 20 did the Swift  $U$ -band magnitude reach 18.02, which would correspond to 2.9 counts  $s^{-1}$  in the OM light curve, off the scale in Figure 4.

The XMM-Newton observation is the first to cover the entire orbit in X-rays with sensitivity sufficient to characterize the light curve at any flux level previously detected by Swift. It shows nearly continuous flaring at all orbital phases superposed on a broad trend that is consistent with intrabinary shock models. However, as best illustrated by Figure 5 the stochastic nature of the flares makes it impossible to define any underlying “qui-

<sup>5</sup> <https://xmmweb.esac.esa.int/docs/documents/CAL-TN-0019.pdf>

escent” light curve precisely. The minimum is evidently near phase  $\phi = 0.25$ , but the broad maximum may or may not be centered at  $\phi = 0.75$ , the inferior conjunction of the pulsar. Instead, there may be a plateau that slopes downward from  $\phi = 0.6$  to  $\phi = 1$ , a common asymmetry in redbacks, e.g., PSR J1023+0038 (Bogdanov et al. 2011), PSR J2215+5135 (Sullivan & Romani 2024), and PSR J2129–0429 (Romani & Sanchez 2016). In any case, such light curves are generally modeled with a shock that is wrapped around the pulsar, with synchrotron emission beamed by particles that flow tangentially to the shock surface (Romani & Sanchez 2016; Wadiasingh et al. 2017, 2018; Kandel et al. 2019; van der Merwe et al. 2020). The persistence of flaring through  $\phi = 0.25$  suggests that a major fraction of the emitting region is not eclipsed by the companion.

The low- and high-flux phases in Table 2 have  $F_X(0.3 - 10 \text{ keV}) = 4.3 \times 10^{-13}$  and  $6.6 \times 10^{-13}$  erg cm $^{-2}$  s $^{-1}$ , respectively. In the context of the Swift monitoring results, this is the “intermediate state” as categorized in Paper 1, while the low flux state in Swift had on average  $F_X(0.3 - 8 \text{ keV}) = 1.95 \times 10^{-13}$  erg cm $^{-2}$  s $^{-1}$ . This suggests that 1FGL J0523.5–2529 may flare continuously in X-rays, stopping only in its lowest state, where its X-ray flux is less than half of the present XMM-Newton observed value. A straight extrapolation of the X-ray power-law spectrum to UV and optical frequencies fails to account for even the small excess of OM counts above the ellipsoidal contribution, since it corresponds to  $U = 24.0$  (before applying interstellar extinction) at 3440Å, the center of the OM  $U$  band. Even during the peak of the brightest flares observed by Swift in 2020, the UV to X-ray spectral energy distribution of the flare must have been steeper than the X-ray spectrum alone; see Paper 1 for details.

The phase-averaged X-ray luminosity of  $3.3 \times 10^{32}$  erg s $^{-1}$  and spectral index  $\Gamma = 1.53$  are close to the mean values for redbacks:  $2.3 \times 10^{32}$  erg s $^{-1}$  and  $\Gamma = 1.44$  (Swihart et al. 2022). In comparison, the brightest flare previously seen by Swift in 2020 had a peak luminosity of  $\approx 8 \times 10^{33}$  erg s $^{-1}$ . Although the spin-down power  $\dot{E}$  of 1FGL J0523.5–2529 is unknown, the mean ratio  $L_x/\dot{E}$  for redbacks is  $\approx 2 \times 10^{-3}$ , which would suggest that  $\dot{E} \sim 10^{35}$  erg s $^{-1}$ .

The power-law spectral index is close to 1.5, the smallest that is likely to be produced by diffusive shock acceleration, and shows no change between the opposite phases of the orbit. Neither is there evidence for thermal plasma emission, either bremsstrahlung or emission lines, in the residuals from the spectral fit. Similar and even flatter indices in redbacks support the theory that magnetic reconnection accelerates the synchrotron emit-

ting particles (Sironi & Spitkovsky 2011; Cortés & Sironi 2022), in this case without evidence of reprocessing of energy into hot plasma. The bright flares in 2020–2021, on the other hand, had a steeper spectrum in the optical through far UV that was not constrained well enough to rule out a thermal contribution, especially in the unobserved extreme UV.

#### 4.2. Absence of Radio Pulsations

Many redbacks are difficult to detect as radio pulsars because they are eclipsed during half or more of the orbit and also randomly disappear at any orbital phase (e.g., Perez et al. 2023, and references therein). 1FGL J0523.5–2529 has been searched unsuccessfully for pulsations at all orbital phases (Johnson et al. 2025). Redbacks and BWs that flare frequently and have strong, variable recombination emission lines are the most elusive, suggesting that these properties, which they share with 1FGL J0523.5–2529 are signatures of dense plasma that can scatter or absorb radio pulses. One such reback candidate was 3FGL J0838.8–2829 (Halpern et al. 2017b; Cho et al. 2018), which was only confirmed as PSR J0838–2827 (Thongmeekom et al. 2024) after several unsuccessful radio campaigns. It was then possible to bootstrap the entire coherent pulse timing history from Fermi. Another reback candidate comes from radio imaging of 4FGL J1646.5–4406 (Zic et al. 2024). It is totally eclipsed during 40% of its 5.27 hr (presumed) orbital period, implying a radius of the absorbing medium larger than the likely size of a companion star’s Roche lobe. It was not detected as a pulsar even out of eclipse, possibly due to dispersion or scattering by an extended wind.

Among BW and BW candidates, a small fraction are not detected as radio pulsars. The one BW that is most similar to 1FGL J0523.5–2529 in its behavior is PSR J1311–3430, which flares frequently in X-ray and optical/UV (Romani 2012; An et al. 2017; De Luca et al. 2022) at all phases and has strong emission lines (Romani et al. 2015). In one XMM-Newton observation, six X-ray flares recurred with a period of 124 minutes, different from the orbital period of 93.77 minutes. Its 2.56 ms pulsations were first detected in a blind search of the Fermi  $\gamma$ -rays (Pletsch et al. 2012), and only later in radio (Ray et al. 2013) with the help of the  $\gamma$ -ray ephemeris. Even then, only one weak detection lasting  $\approx 1100$  s was achieved during a total of 22.25 hr of exposure over 20 sessions. The lesson from these highly enshrouded pulsars is that many repeated observations at different frequencies may eventually encounter a temporary hole through which radio pulses escape, enough to seed a comprehensive Fermi timing solution.

### 4.3. Interpretation

Observations of 1FGL J0523.5–2529 indicate that its companion is the source of a substantial stellar wind that encloses the pulsar with plasma that absorbs any radio pulsations, generates variable recombination emission lines, and emits nonthermal, persistent and flaring X-rays when shocked against the pulsar wind. These phenomena suggest an interpretation in terms of the conditions for pressure balance and shock stability investigated by [Wadiasingh et al. \(2018\)](#) in the case of a shock curved around the pulsar, which we recount here. For a companion wind to be wrapped around the pulsar, it should be gravitationally captured within the Roche lobe of the pulsar, losing angular momentum but not circularizing before reaching the shock, else an accretion disk would form. This requires viscosity and heating within the pulsar’s Roche lobe, i.e., an advection-dominated accretion flow upstream of the shock.

However, such a shock configuration is unstable on a dynamical (orbital) timescale, requiring some regulating effect, e.g., irradiation of the companion, to stabilize it on the longer timescales it is observed to exist. This suggested to [Wadiasingh et al. \(2018\)](#) that all redbacks with shocks curved around the pulsar are transitional MSPs (tMSPs), in which the intrabinary shock alternates on timescales of years to decades with a subluminous accretion disk displaying a distinctive set of phenomena unlike 1FGL J0523.5–2529. See, e.g., the prototype tMSP PSR J1023+0038 ([Bogdanov et al. 2015](#)). Variable irradiation feedback on stars that are convection-dominated in their energy transport is likely to induce expansion or contraction of the stellar envelope with little change in effective temperature, thus, an inverse correlation of luminosity with radius. In this interpretation, the decrease in the optical brightness of 1FGL J0523.5–2529 observed over the past 10 years indicates an increasing Roche-lobe filling fraction that may allow the mass-loss rate or circularization radius to increase, predicting an eventual transition to the accretion-disk state, for which there is no evidence yet (Paper 1).

The dynamical time scale may be relevant to the observed flares, with rise times of  $\sim 5$  minutes and durations of  $\sim 30$  minutes. The semi-major axis of the binary is  $\approx 3 \times 10^{11}$  cm according to the orbital parameters of [Strader et al. \(2019\)](#). At a radius  $r \approx 8 \times 10^{10}$  cm from the pulsar, well within its Roche lobe, the dynamical time  $\sqrt{r^3/GM_p}$  is also  $\sim 30$  minutes. If there are density inhomogeneities in the wind that enhance the shocked luminosity, this could represent the time for the largest such structures to pass through the shock or leave the region of enhanced magnetic field in which they radiate.

## 5. CONCLUSIONS

The first X-ray observation to study the highly variable candidate redback 1FGL J0523.5–2529 over its entire 16.5 hr orbit finds it at an average flux  $\approx 2$  times greater than the poorly characterized minimum that Swift measured previously. The X-ray spectrum is consistent with a power law of  $\Gamma = 1.53$ , independent of the orbital phase, and similar to that of other redbacks. The most notable new result is the prevalence of flares, but only  $\approx 0.02$  times as luminous as the rare bright flares that first distinguished this object in 2020. These small flares make it difficult to study the quiescent structure of the underlying intrabinary shock, if it even has a stable configuration emitting at half the present flux or less. Because a broad minimum in the flux is centered at the inferior conjunction of the putative pulsar as determined by prior optical spectroscopy and continued photometry of the companion star, the shock most likely is wrapped around the pulsar. The simultaneous *U*-band light curve from the OM is dominated by ellipsoidal modulation of the photospheric emission of the bright companion star, consistent with previous ground-based optical and Swift photometry.

The failure to detect radio pulsations from 1FGL J0523.5–2529 may be related to the unusually massive companion (for a redback). Its Roche lobe presents a large target for the pulsar wind, which might help to generate a strong stellar wind capable of enshrouding the pulsar and absorbing or scattering radio pulses, while the flares may be evidence of inhomogeneities in the shocked wind.

## ACKNOWLEDGEMENTS

This investigation is based on an observation made by XMM-Newton, an ESA science mission with instruments and contributions directly funded by ESA Member States and NASA, and includes data obtained at the MDM Observatory, operated by Dartmouth College, Columbia University, The Ohio State University, Ohio University, and the University of Michigan. Support for this work was provided by NASA XMM-Newton guest observer grant 80NSSC24K1517. The Zwicky Transient Facility is supported by the National Science Foundation under Grants No. AST-1440341 and AST-2034437 and a collaboration including current partners Caltech, IPAC, the Oskar Klein Center at Stockholm University, the University of Maryland, University of California, Berkeley, the University of Wisconsin at Milwaukee, University of Warwick, Ruhr University, Cornell University, Northwestern University and Drexel University. Operations are conducted by COO, IPAC, and UW. The

ATLAS project is primarily funded to search for near earth asteroids through NASA grants NN12AR55G, 80NSSC18K0284, and 80NSSC18K1575. The ATLAS science products have been made possible through the contributions of the University of Hawaii Institute for Astronomy, the Queen's University Belfast, the Space Telescope Science Institute, the South African Astronomical Observatory, and The Millennium Institute of Astrophysics (MAS), Chile. The XMM-Newton Science Analysis Software (SAS) is developed and maintained by the Science Operations Centre at the European Space Astronomy Centre and the Survey Science Centre at the University of Leicester. This research has made use of

data and software provided by the High Energy Astrophysics Science Archive Research Center (HEASARC), which is a service of the Astrophysics Science Division at NASA/GSFC. We acknowledge use of NASA's Astrophysics Data System (ADS) Bibliographic Services and the arXiv.

*Facilities:* ATLAS, McGraw-Hill, XMM

*Software:* HEASoft (Nasa High Energy Astrophysics Science Archive Research Center (Heasarc) 2014), SAS (Gabriel et al. 2004)

## REFERENCES

- Al Noori, H., Roberts, M. S. E., Torres, R. A., et al. 2018, ApJ, 861, 89, doi: [10.3847/1538-4357/aac828](https://doi.org/10.3847/1538-4357/aac828)
- Alpar, M. A., Cheng, A. F., Ruderman, M. A., & Shaham, J. 1982, Nature, 300, 728, doi: [10.1038/300728a0](https://doi.org/10.1038/300728a0)
- An, H., Romani, R. W., Johnson, T., Kerr, M., & Clark, C. J. 2017, ApJ, 850, 100, doi: [10.3847/1538-4357/aa947f](https://doi.org/10.3847/1538-4357/aa947f)
- Bellm, E. C., Kaplan, D. L., Breton, R. P., et al. 2016, ApJ, 816, 74, doi: [10.3847/0004-637X/816/2/74](https://doi.org/10.3847/0004-637X/816/2/74)
- Bellm, E. C., Kulkarni, S. R., Graham, M. J., et al. 2019, PASP, 131, 018002, doi: [10.1088/1538-3873/aaeabe](https://doi.org/10.1088/1538-3873/aaeabe)
- Bogdanov, S., Archibald, A. M., Hessels, J. W. T., et al. 2011, ApJ, 742, 97, doi: [10.1088/0004-637X/742/2/97](https://doi.org/10.1088/0004-637X/742/2/97)
- Bogdanov, S., Grindlay, J. E., & van den Berg, M. 2005, ApJ, 630, 1029, doi: [10.1086/432249](https://doi.org/10.1086/432249)
- Bogdanov, S., Patruno, A., Archibald, A. M., et al. 2014, ApJ, 789, 40, doi: [10.1088/0004-637X/789/1/40](https://doi.org/10.1088/0004-637X/789/1/40)
- Bogdanov, S., Archibald, A. M., Bassa, C., et al. 2015, ApJ, 806, 148, doi: [10.1088/0004-637X/806/2/148](https://doi.org/10.1088/0004-637X/806/2/148)
- Cho, P. B., Halpern, J. P., & Bogdanov, S. 2018, ApJ, 866, 71, doi: [10.3847/1538-4357/aade92](https://doi.org/10.3847/1538-4357/aade92)
- Claret, A., & Bloemen, S. 2011, A&A, 529, A75, doi: [10.1051/0004-6361/201116451](https://doi.org/10.1051/0004-6361/201116451)
- Cortés, J., & Sironi, L. 2022, ApJ, 933, 140, doi: [10.3847/1538-4357/ac74b2](https://doi.org/10.3847/1538-4357/ac74b2)
- . 2024, MNRAS, 534, 2551, doi: [10.1093/mnras/stae2278](https://doi.org/10.1093/mnras/stae2278)
- . 2025, MNRAS, 542, 917, doi: [10.1093/mnras/staf284](https://doi.org/10.1093/mnras/staf284)
- De Luca, A., Marelli, M., Mereghetti, S., et al. 2022, A&A, 667, L7, doi: [10.1051/0004-6361/202244643](https://doi.org/10.1051/0004-6361/202244643)
- Deneva, J. S., Ray, P. S., Camilo, F., et al. 2016, ApJ, 823, 105, doi: [10.3847/0004-637X/823/2/105](https://doi.org/10.3847/0004-637X/823/2/105)
- . 2021, ApJ, 909, 6, doi: [10.3847/1538-4357/abd7a1](https://doi.org/10.3847/1538-4357/abd7a1)
- Drake, A. J., Djorgovski, S. G., Mahabal, A., et al. 2009, ApJ, 696, 870, doi: [10.1088/0004-637X/696/1/870](https://doi.org/10.1088/0004-637X/696/1/870)
- Eastman, J., Siverd, R., & Gaudi, B. S. 2010, PASP, 122, 935, doi: [10.1086/655938](https://doi.org/10.1086/655938)
- Gabriel, C., Denby, M., Fyfe, D. J., et al. 2004, in Astronomical Society of the Pacific Conference Series, Vol. 314, Astronomical Data Analysis Software and Systems (ADASS) XIII, ed. F. Ochsenbein, M. G. Allen, & D. Egret, 759
- Gaia Collaboration, Brown, A. G. A., Vallenari, A., et al. 2021, A&A, 649, A1, doi: [10.1051/0004-6361/202039657](https://doi.org/10.1051/0004-6361/202039657)
- Gomel, R., Faigler, S., & Mazeh, T. 2021, MNRAS, 501, 2822, doi: [10.1093/mnras/staa3305](https://doi.org/10.1093/mnras/staa3305)
- Halpern, J. P., Bogdanov, S., & Thorstensen, J. R. 2017a, ApJ, 838, 124, doi: [10.3847/1538-4357/838/2/124](https://doi.org/10.3847/1538-4357/838/2/124)
- Halpern, J. P., Perez, K. I., & Bogdanov, S. 2022, ApJ, 935, 151, doi: [10.3847/1538-4357/ac8161](https://doi.org/10.3847/1538-4357/ac8161)
- Halpern, J. P., Strader, J., & Li, M. 2017b, ApJ, 844, 150, doi: [10.3847/1538-4357/aa7c6f](https://doi.org/10.3847/1538-4357/aa7c6f)
- HI4PI Collaboration, Ben Bekhti, N., Flöer, L., et al. 2016, A&A, 594, A116, doi: [10.1051/0004-6361/201629178](https://doi.org/10.1051/0004-6361/201629178)
- Johnson, O. A., Keane, E. F., McKenna, D. J., et al. 2025, The Open Journal of Astrophysics, 8, 47516, doi: [10.33232/001c.147516](https://doi.org/10.33232/001c.147516)
- Kandel, D., Romani, R. W., & An, H. 2019, ApJ, 879, 73, doi: [10.3847/1538-4357/ab24d9](https://doi.org/10.3847/1538-4357/ab24d9)
- Koljonen, K. I. I., & Linares, M. 2025, ApJ, 994, 8, doi: [10.3847/1538-4357/ae08a5](https://doi.org/10.3847/1538-4357/ae08a5)
- Li, M., Halpern, J. P., & Thorstensen, J. R. 2014, ApJ, 795, 115, doi: [10.1088/0004-637X/795/2/115](https://doi.org/10.1088/0004-637X/795/2/115)
- Mason, K. O., Breeveld, A., Much, R., et al. 2001, A&A, 365, L36, doi: [10.1051/0004-6361:20000044](https://doi.org/10.1051/0004-6361:20000044)
- Morris, S. L., & Naftilan, S. A. 1993, ApJ, 419, 344, doi: [10.1086/173488](https://doi.org/10.1086/173488)
- Nasa High Energy Astrophysics Science Archive Research Center (Heasarc). 2014, HEASoft: Unified Release of FTOOLS and XANADU, Astrophysics Source Code Library, record ascl:1408.004. <http://ascl.net/1408.004>

- Perez, K. I., Bogdanov, S., Halpern, J. P., & Gajjar, V. 2023, *ApJ*, 952, 150, doi: [10.3847/1538-4357/acdc23](https://doi.org/10.3847/1538-4357/acdc23)
- Pletsch, H. J., Guillemot, L., Fehrmann, H., et al. 2012, *Science*, 338, 1314, doi: [10.1126/science.1229054](https://doi.org/10.1126/science.1229054)
- Radhakrishnan, V., & Srinivasan, G. 1982, *Current Science*, 51, 1096
- Ray, P. S., Ransom, S. M., Cheung, C. C., et al. 2013, *ApJL*, 763, L13, doi: [10.1088/2041-8205/763/1/L13](https://doi.org/10.1088/2041-8205/763/1/L13)
- Rea, N., Coti Zelati, F., Esposito, P., et al. 2017, *MNRAS*, 471, 2902, doi: [10.1093/mnras/stx1560](https://doi.org/10.1093/mnras/stx1560)
- Romani, R. W. 2012, *ApJL*, 754, L25, doi: [10.1088/2041-8205/754/2/L25](https://doi.org/10.1088/2041-8205/754/2/L25)
- Romani, R. W., Filippenko, A. V., & Cenko, S. B. 2015, *ApJ*, 804, 115, doi: [10.1088/0004-637X/804/2/115](https://doi.org/10.1088/0004-637X/804/2/115)
- Romani, R. W., & Sanchez, N. 2016, *ApJ*, 828, 7, doi: [10.3847/0004-637X/828/1/7](https://doi.org/10.3847/0004-637X/828/1/7)
- Sanchez, N., & Romani, R. W. 2017, *ApJ*, 845, 42, doi: [10.3847/1538-4357/aa7a02](https://doi.org/10.3847/1538-4357/aa7a02)
- Shahbaz, T., Linares, M., & Breton, R. P. 2017, *MNRAS*, 472, 4287, doi: [10.1093/mnras/stx2195](https://doi.org/10.1093/mnras/stx2195)
- Sironi, L., & Spitkovsky, A. 2011, *ApJ*, 741, 39, doi: [10.1088/0004-637X/741/1/39](https://doi.org/10.1088/0004-637X/741/1/39)
- Strader, J., Chomiuk, L., Sonbas, E., et al. 2014, *ApJL*, 788, L27, doi: [10.1088/2041-8205/788/2/L27](https://doi.org/10.1088/2041-8205/788/2/L27)
- Strader, J., Swihart, S., Chomiuk, L., et al. 2019, *ApJ*, 872, 42, doi: [10.3847/1538-4357/aafbaa](https://doi.org/10.3847/1538-4357/aafbaa)
- Strüder, L., Briel, U., Dennerl, K., et al. 2001, *A&A*, 365, L18, doi: [10.1051/0004-6361:20000066](https://doi.org/10.1051/0004-6361:20000066)
- Sullivan, A. G., & Romani, R. W. 2024, *ApJ*, 974, 315, doi: [10.3847/1538-4357/ad4d85](https://doi.org/10.3847/1538-4357/ad4d85)
- Swihart, S. J., Strader, J., Chomiuk, L., et al. 2022, *ApJ*, 941, 199, doi: [10.3847/1538-4357/aca2ac](https://doi.org/10.3847/1538-4357/aca2ac)
- Thongmeearkom, T., Clark, C. J., Breton, R. P., et al. 2024, *MNRAS*, 530, 4676, doi: [10.1093/mnras/stae787](https://doi.org/10.1093/mnras/stae787)
- Tonry, J. L., Denneau, L., Heinze, A. N., et al. 2018, *PASP*, 130, 064505, doi: [10.1088/1538-3873/aabadf](https://doi.org/10.1088/1538-3873/aabadf)
- Torres, G. 2021, *Research Notes of the American Astronomical Society*, 5, 256, doi: [10.3847/2515-5172/ac34ef](https://doi.org/10.3847/2515-5172/ac34ef)
- Turner, M. J. L., Abbey, A., Arnaud, M., et al. 2001, *A&A*, 365, L27, doi: [10.1051/0004-6361:20000087](https://doi.org/10.1051/0004-6361:20000087)
- van der Merwe, C. J. T., Wadiasingh, Z., Venter, C., Harding, A. K., & Baring, M. G. 2020, *ApJ*, 904, 91, doi: [10.3847/1538-4357/abdbfb](https://doi.org/10.3847/1538-4357/abdbfb)
- van Staden, A. D., & Antoniadis, J. 2016, *ApJL*, 833, L12, doi: [10.3847/2041-8213/833/1/L12](https://doi.org/10.3847/2041-8213/833/1/L12)
- Verner, D. A., Ferland, G. J., Korista, K. T., & Yakovlev, D. G. 1996, *ApJ*, 465, 487, doi: [10.1086/177435](https://doi.org/10.1086/177435)
- Wadiasingh, Z., Harding, A. K., Venter, C., Böttcher, M., & Baring, M. G. 2017, *ApJ*, 839, 80, doi: [10.3847/1538-4357/aa69bf](https://doi.org/10.3847/1538-4357/aa69bf)
- Wadiasingh, Z., Venter, C., Harding, A. K., Böttcher, M., & Kilian, P. 2018, *ApJ*, 869, 120, doi: [10.3847/1538-4357/aaed43](https://doi.org/10.3847/1538-4357/aaed43)
- Wilms, J., Allen, A., & McCray, R. 2000, *ApJ*, 542, 914, doi: [10.1086/317016](https://doi.org/10.1086/317016)
- Zic, A., Wang, Z., Lenc, E., et al. 2024, *MNRAS*, 528, 5730, doi: [10.1093/mnras/stae033](https://doi.org/10.1093/mnras/stae033)
- Zyuzin, D. A., Kirichenko, A. Y., Karpova, A. V., et al. 2024, *MNRAS*, 527, 6712, doi: [10.1093/mnras/stad3552](https://doi.org/10.1093/mnras/stad3552)